Equilibrium orientations and positions of non-spherical particles in optical traps

Yongyin Cao,[1,2,*] Alexander B Stilgoe,[2] Lixue Chen,[1] Timo A Nieminen,[2] and Halina Rubinsztein-Dunlop[2]

[1]*Department of Physics, School of Science, Harbin Institute of Technology, Harbin, 150001, China*
[2]*School of Mathematics and Physics, The University of Queensland, Brisbane, QLD 4072, Australia*
[*] *yongyincao@gmail.com*

Abstract: Dynamic simulation is a powerful tool to observe the behavior of arbitrary shaped particles trapped in a focused laser beam. Here we develop a method to find equilibrium positions and orientations using dynamic simulation. This general method is applied to micro- and nano-cylinders as a demonstration of its predictive power. Orientation landscapes for particles trapped with beams of differing polarisation are presented. The torque efficiency of micro-cylinders at equilibrium in a plane is also calculated as a function of tilt angle. This systematic investigation elucidates in both the function and properties of micro- and nano-cylinders trapped in optical tweezers.

OCIS codes: (140.7010) Laser trapping; (350.4855) Optical tweezers or optical manipulation.

References and links

1. A. Ashkin, "Acceleration and trapping of particles by radiation pressure," Phys. Rev. Lett. **24**, 156–159 (1970).
2. A. Ashkin, J. M. Dziedzic, J. E. Bjorkholm, and S. Chu, "Observation of a single-beam gradient force optical trap for dielectric particles," Opt. Lett. **11**(5), 288–290 (1986).
3. J. Harris and G. McConnell, "Optical trapping and manipulation of live T cells with a low numerical aperture lens," Opt. Express **16**(18), 14036–14043 (2008).
4. M. C. Zhong, J. H. Zhou, Y. X. Ren, Y. M. Li, and Z. Q. Wang, "Rotation of birefringent particles in optical tweezers with spherical aberration," Appl. Opt. **48**(22), 4397–4402 (2009).
5. M. Rodriguez-Otazo, A. Augier-Calderin, J. P. Galaup, J. F. Lamère, and S. Fery-Forgues, "High rotation speed of single molecular microcrystals in an optical trap with elliptically polarized light," Appl. Opt. **48**(14), 2720–2730 (2009).
6. A. Mazolli, P. A. Maia Neto, and H. M. Nussenzveig, "Theory of trapping forces in optical tweezers," Proc. R. Soc. Lond. A **459**, 3021–3041 (2003).
7. T. A. Nieminen, V. L. Y. Loke, A. B. Stilgoe, G. Knöner, A. M. Brańczyk, N. R. Heckenberg, and H. Rubinsztein-Dunlop, "Optical tweezers computational toolbox," J. Opt. A **9**, S196–S203 (2007).
8. A. A. R. Neves, A. Fontes, Lde. Y. Pozzo, A. A. de Thomaz, E. Chillce, E. Rodriguez, L. C. Barbosa, and C. L. Cesar, "Electromagnetic forces for an arbitrary optical trapping of a spherical dielectric," Opt. Express **14**(26), 13101–13106 (2006).
9. G. Knöner, T. A. Nieminen, S. Parkin, N. R. Heckenberg, and H. Rubinsztein-Dunlop, "Calculation of optical trapping landscapes," Proc. SPIE **6326**, U119–U127 (2006).
10. A. B. Stilgoe, T. A. Nieminen, G. Knöener, N. R. Heckenberg, and H. Rubinsztein-Dunlop, "The effect of Mie resonances on trapping in optical tweezers," Opt. Express **16**(19), 15039–15051 (2008).
11. T. A. Nieminen, T. Asavei, V. L. Y. Loke, N. R. Heckenberg, and H. Rubinsztein-Dunlop, "Symmetry and the generation and measurement of optical torque," J. Quant. Spectrosc. Radiat. Transf. **110**, 1472–1482 (2009).
12. R. C. Gauthier, "Trapping model for the low-index ring-shaped micro-object in a focused, lowest-order Gaussian laser-beam profile," J. Opt. Soc. Am. B **14**, 782–789 (1997).
13. R. C. Gauthier, "Theoretical investigation of the optical trapping force and torque on cylindrical micro-objects," J. Opt. Soc. Am. B **14**, 3323–3333 (1997).
14. K. Ramser and D. Hanstorp, "Optical manipulation for single-cell studies," J Biophoton. **3**(4), 187–206 (2010).
15. R. C. Gauthier and A. Frangioudakis, "Theoretical investigation of the optical trapping properties of a micro-optic cubic glass structure," Appl. Opt. **39**(18), 3060–3070 (2000).
16. H. Ukita and H. Kawashima, "Optical rotor capable of controlling clockwise and counterclockwise rotation in optical tweezers by displacing the trapping position," Appl. Opt. **49**(10), 1991–1996 (2010).
17. P. H. Jones, F. Palmisano, F. Bonaccorso, P. G. Gucciardi, G. Calogero, A. C. Ferrari, and O. M. Maragó, "Rotation Detection in Light-Driven Nanorotors," ACS Nano **3**(10), 3077–3084 (2009).
18. T. A. Nieminen, V. L. Y. Loke, A. B. Stilgoe, N. R. Heckenberg, and H. Rubinsztein-Dunlop, "T-matrix method for modelling optical tweezers," J. Mod. Opt. **58**, 528–544 (2011).

#164286 - $15.00 USD Received 7 Mar 2012; revised 3 May 2012; accepted 4 May 2012; published 24 May 2012

19. V. L. Y. Loke, T. A. Nieminen, N. R. Heckenberg, and H. Rubinsztein-Dunlop, "T-matrix calculation via discrete dipole approximation, point matching and exploiting symmetry," J. Quant. Spectrosc. Radiat. Transf. **110**, 1460–1471 (2009).
20. S. H. Simpson and S. Hanna, "Application of the discrete dipole approximation to optical trapping calculations of inhomogeneous and anisotropic particles," Opt. Express **19**(17), 16526–16541 (2011).
21. P. C. Chaumet and C. Billaudeau, "Coupled dipole method to compute optical torque: Application to a micro-propeller," J. Appl. Phys. **101**, 023106 (2007).
22. S. D. Tan, H. A. Lopez, C. W. Cai, and Y. G. Zhang, "Optical trapping of single-walled carbon nanotubes," Nano Lett. **4**, 1415–1419 (2004).
23. J. L. Zhang, T. G. Kim, S. C. Jeoung, F. F. Yao, H. Lee, and X. D. Sun, "Controlled trapping and rotation of carbon nanotube bundle with optical tweezers," Opt. Commun. **267**, 260–263 (2006).
24. Y. Nakayama, P. J. Pauzauskie, A. Radenovic, R. M. Onorato, R. J. Saykally, J. Liphardt, and P. D. Yang, "Tunable nanowire nonlinear optical probe," Nature **447**(7148), 1098–1101 (2007).
25. A. A. R. Neves, A. Camposeo, S. Pagliara, R. Saija, F. Borghese, P. Denti, M. A. Iatì, R. Cingolani, O. M. Maragò, and D. Pisignano, "Rotational dynamics of optically trapped nanofibers," Opt. Express **18**(2), 822–830 (2010).
26. F. Borghese, P. Denti, R. Saija, M. A. Iatì, and O. M. Maragò, "Radiation torque and force on optically trapped linear nanostructures," Phys. Rev. Lett. **100**(16), 163903 (2008).
27. S. H. Simpson and S. Hanna, "Holographic optical trapping of microrods and nanowires," J. Opt. Soc. Am. A **27**(6), 1255–1264 (2010).
28. M. Dienerowitz, M. Mazilu, and K. Dholakia, "Optical manipulation of nanoparticles: a review," J. Nanophoton. **2**, 021875 (2008).
29. T. A. Nieminen, N. R. Heckenberg, and H. Rubinsztein-Dunlop, "Calculation of the T-matrix: general considerations and application of the point-matching method," J. Quant. Spectrosc. Radiat. Transf. **79–80**, 1019–1029 (2003).
30. A. I. Bishop, T. A. Nieminen, N. R. Heckenberg, and H. Rubinsztein-Dunlop, "Optical application and measurement of torque on microparticles of isotropic nonabsorbing material," Phys. Rev. A **68**, 033802 (2003).
31. C. H. Choi, J. Ivanic, M. S. Gordon, and K. Ruedenberg, "Rapid and stable determination of rotation matrices between spherical harmonics by direct recursion," J. Chem. Phys. **111**, 8825–8831 (1999).
32. O. A. Bauchau and L. Trainelli, "The vectorial parameterization of rotation," Nonlinear Dyn. **32**, 71–92 (2003).
33. E. M. Purcell, "Life at low Reynolds-number," Am. J. Phys. **45**, 3–11 (1977).
34. J. G. Garcia de la Torre and V. A. Bloomfield, "Hydrodynamic properties of complex, rigid, biological macromolecules: theory and applications," Q. Rev. Biophys. **14**(1), 81–139 (1981).
35. T. A. Nieminen, H. Rubinsztein-Dunlop, N. R. Heckenberg, and A. I. Bishop, "Numerical modelling of optical trapping," Comput. Phys. Commun. **142**, 468–471 (2001).
36. S. Albaladejo, M. I. Marqués, M. Laroche, and J. J. Sáenz, "Scattering forces from the curl of the spin angular momentum of a light field," Phys. Rev. Lett. **102**(11), 113602 (2009).
37. H. K. Moffat, "Six Lectures on General Fluid Dynamics and Two on Hydromagnetic Dynamo Theory," in *Fluid Dynamics*, R. Balian and J.-L. Peube eds., (Gordon and Breach, 1977), pp. 149–234.

1. Introduction

In the early part of 1970s [1], Ashkin and associates reported that a single microsphere can be suspended against gravity by a focused laser beam, and also showed that the sphere can be trapped in the focal region of two perfectly aligned counter-propagating laser beams. In 1986, Ashkin et al. [2] demonstrated that a single tightly focused laser beam can trap a microsphere in three dimensions in the waist of a highly focused beam. Since the pioneering work of Ashkin, laser-based trapping and manipulation of particles has found widespread use in fields of biology, physics, and chemistry [3–5]. Microspheres have continued to be popular objects of optical trapping, being widely used as handles or probes. The simple geometry of microspheres allows computational modelling of optical tweezers using generalized Lorenz-Mie theory [6–8]. Where such a particle is trapped using a Gaussian beam, it is known beforehand that the equilibrium will lie on the beam axis, and the most important properties of the trap, such as the axial and radial trap strengths and spring constants can be calculated. Such calculations can be performed efficiently enough to explore the dependence on parameters such as particle size, refractive index, the numerical aperture of the focussing lens, or other parameters [6,8–10]. More general calculations can be performed, for example to find the optical force as a function of position. This can be carried out over a closely-spaced three-dimensional grid (or two-dimensional for circularly polarized beams).

However, not all particles that are trapped or manipulated in optical traps are spherical. Particles such as crystals and bacteria or other single cells can be non-spherical, or we can choose to fabricate non-spherical particles for specific purposes, such as to exert optical torques [11]. Non-spherical particles that have been investigated include: rings [12], cylinders

#164286 - $15.00 USD Received 7 Mar 2012; revised 3 May 2012; accepted 4 May 2012; published 24 May 2012

[13], single cells [14], cubes [15], and microrotors [16,17]. Characterization of the trapping of such particles by computational modelling is significantly more difficult than for spherical particles. The first difficulty is that, unlike the analytical solution for spheres, it is necessary to resort to numerical methods to solve the scattering problem. A number of methods are known to be useful for modelling optical trapping, for example, using the T-matrix method. One of the most flexible, as far as particle geometry is concerned, is the discrete dipole approximation, or DDA (also known as the coupled-dipole method) [18–21]. The second difficulty is that the non-spherical shape introduces two (for axisymmetric particles) or three degrees of freedom, required to describe the orientation of the particle. Since, for a single particle, this results in a total of 4 (for axisymmetric particles in circularly polarized Gaussian beams), 5, or 6 degrees of freedom, the computational time required to calculate the force over a sufficiently fine grid becomes excessive. In addition, it is no longer certain that the particle is centred on the beam axis in the equilibrium position. An alternative approach is required. Noting that if a particle is introduced into an optical trap, it will "fall" into its equilibrium position and orientation, we see that if we model this process, we can readily find the equilibrium position and orientation of a particle. This requires us to calculate the optical force and torque, and the translational and rotational viscous drag force and torque, and model the motion of the particle as it moves into the trap. This can be done with far fewer calculations than required to characterize the trap as a function of the degrees of freedom (particle position and orientation).

One interesting class of non-spherical particles is elongated nanoparticles, such as carbon nanotubes [22,23], semiconductor nanowires [24], and nanofibers [25]. Such particles often have subwavelength cross-sections. Optical trapping and manipulation of non-spherical nanoparticles have been observed in aqueous environments. Recently, radiation torque and trapping force on optically trapped linear nanostructures has been studied by F. Borghese et al. [26]. The holographic optical trapping of nanowires has been calculated by Stephen H. Simpson et al. [27] using the T-matrix method. Nanoparticle trapping is challenging with optical tweezers and they offer ample new phenomena to explore [28], thus, it is of great importance to investigate the behavior of trapped nanostructures and to discuss their orientation and rotation. Dynamic simulation can rapidly provide information on beam-particle systems without having to interpret conventional force and torque versus position and orientation curves. Here we develop this model and apply it to micro- and nano-cylinders. Figure 1 shows the dynamic simulation for a microcylinder trapped in a single tightly Gaussian beam propagating along z-axis. The cylinder for all starting positions and orientations considered here is finally trapped at the same position with the orientation along the beam axis. A movie of those translations and rotations of the cylinder has been made and is included as supplementary material, from which one can easily observe motion of the cylinder. In this paper, we calculate the force and torque on dielectric cylinders illuminated by a tightly focused laser beam, and study their translation and rotation dynamics. The trapping force and torque exerted on dielectric cylinders are calculated using a numerical method based on discrete dipole approximation (DDA) and tangential field point-matching [29]. The equilibrium positions and stable orientations of micro- and nano-cylinders are obtained using a dynamic simulation model incorporating the translational and rotational friction tensors.

#164286 - $15.00 USD Received 7 Mar 2012; revised 3 May 2012; accepted 4 May 2012; published 24 May 2012

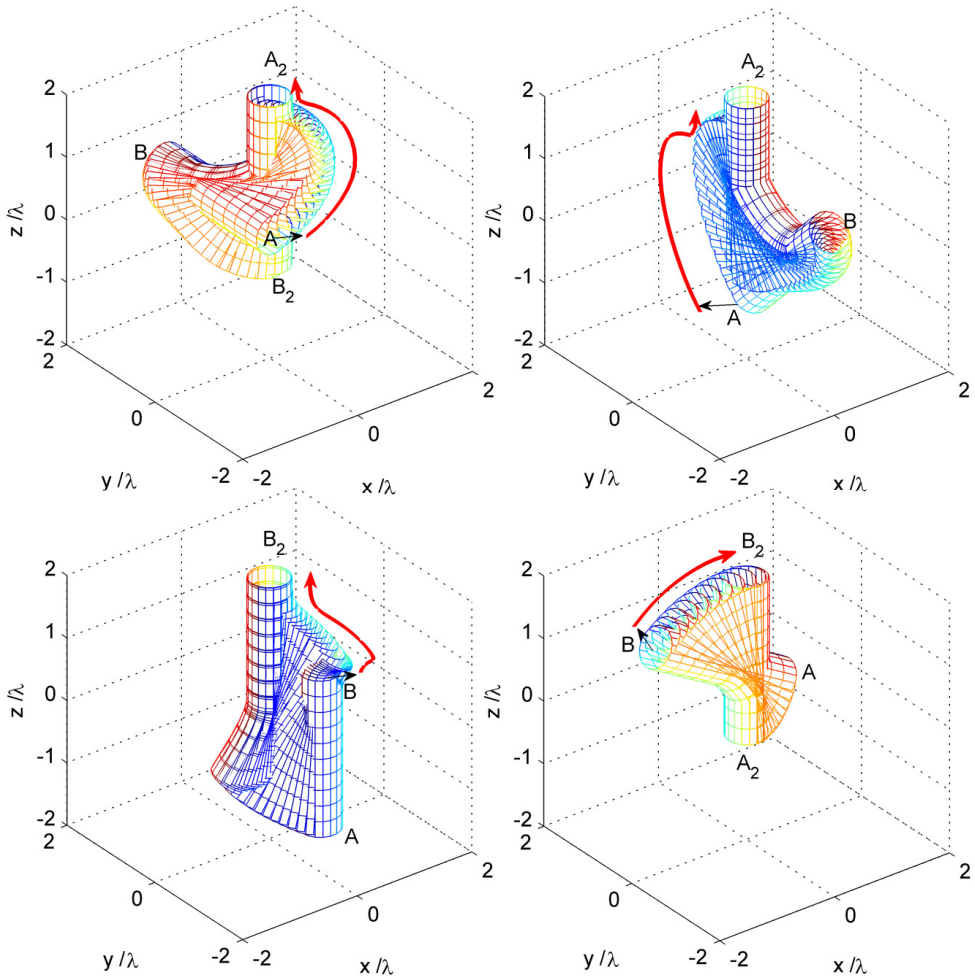

Fig. 1. Trajectories of a glass microcylinder with D = 500 nm and L = 2000 nm in a linearly polarized beam. AB is starting position and orientation of the microcylinder, A_2B_2 is the trapped position and final orientation. The starting positions are (a) (–0.5, 0.5, –0.5)λ, (b) (0, 1, 0)λ, (c) (0.5, –0.5, –0.5)λ and (d) (–0.5, 0, 1)λ. The initial orientations are (a) (90°, 90°), (b) (45°, 270°), (c) (0°, 0°) and (d) (45°, 180°). The solid curve and arrow show the trajectory of one top center of the cylinder. The cylinder was finally trapped vertically at (0, 0, 0.94) λ (Media 1).

2. Theory

For the purpose of explanation of the dynamic simulation, in this section we will present the theory of our calculations.

2.1. T-matrix calculation

In optical tweezers, the optical forces and torques exerted on particles can be considered as the result of the transfer of linear and angular momentum from the electromagnetic field to the particle. In other words, the linear and angular momentum flux of the beam are changed by light scattering off the particle. Thus, the problem of calculating the forces and torques acting on particles is light scattering problem. In our calculations, optical fields are expanded in terms of incident and scattered field potentials, which can be written in terms of a discrete basis set of functions Ψ_n^{inc} and Ψ_n^{scat}, such that,

#164286 - $15.00 USD Received 7 Mar 2012; revised 3 May 2012; accepted 4 May 2012; published 24 May 2012

$$U_{inc} = \sum_{n}^{\infty} a_n \Psi_n^{inc}, \tag{1}$$

$$U_{scat} = \sum_{k}^{\infty} p_k \Psi_k^{scat}. \tag{2}$$

Where n and k are the radial mode indices, a_n and p_k are the expansion coefficients of incident and scattered fields respectively. The relationship between the incident and scattered fields can be written as a matrix equation

$$\tilde{\mathbf{P}} = \mathbf{T}\tilde{\mathbf{A}}, \tag{3}$$

where $\mathbf{T}$ is the transition matrix. $\tilde{\mathbf{P}}$ and $\tilde{\mathbf{A}}$ are vectors of the beam shape coefficients of incident and scattered fields, respectively [30]. If the incident field and T-matrix of the particle are given, the coefficients of the scattered field can be found. There are a number different ways to calculate T matrix. Our T-matrices are constructed using DDA and point-matching.

2.2. Translation and rotation of beam coefficients

If the beam expansion coefficients in the Cartesian coordinate system centered on the focus of the beam are $\mathbf{a}_0$ and $\mathbf{b}_0$, coefficients in a coordinate system at any position can be found using a linear transformation [18,31],

$$\mathbf{a} = \mathbf{R}_2\left(\mathbf{R}_1^{-1}\mathbf{A}\mathbf{R}_1\mathbf{a}_0 + \mathbf{R}_1^{-1}\mathbf{B}\mathbf{R}_1\mathbf{b}_0\right), \tag{4}$$

$$\mathbf{b} = \mathbf{R}_2\left(\mathbf{R}_1^{-1}\mathbf{B}\mathbf{R}_1\mathbf{a}_0 + \mathbf{R}_1^{-1}\mathbf{A}\mathbf{R}_1\mathbf{b}_0\right). \tag{5}$$

Where $\mathbf{a}$ and $\mathbf{b}$ are the TE/TM modes of $\tilde{A}$. $\mathbf{R_1}$ is the rotation of beam shape coefficients from the $x_1y_1z_1$ frame such that z_1 would point along $\mathbf{O_1O_2}$, as shown in Fig. 2. $\mathbf{A}$ and $\mathbf{B}$ are the translations of beam coefficients in the rotated coordinate system along the direction of $\mathbf{O_1O_2}$. $\mathbf{R_2}$ is the rotation of beam coefficients from the Cartesian coordinate system $x_2y_2z_2$ centered at the particle position to the coordinate system $x_3y_3z_3$ in particle orientated frame. According to Eqs. (4)–(5), as long as the beam coefficients in the coordinate system centered at the focus of the beam are given, the coefficients in an arbitrary coordinate system centered at any position can be found using rotations and translations of beam coefficients. Then the coefficients of the scattered field, $\mathbf{p}$ and $\mathbf{q}$ (the TE/TM modes of $\tilde{P}$), can be found by Eq. (3).

Note that, $\mathbf{R}_1$ is calculated using the direction vector $\mathbf{O}_1\mathbf{O}_2$, $\mathbf{A}$ and $\mathbf{B}$ move the beams between O_1 and O_2. $\mathbf{R}_2$ orients the translated field into a particle orientated frame, which depends on a 3×3 rotation matrix $\mathbf{R_{2,3}}$ of particle. $\mathbf{R_{2,3}}$ is considered as a function of time, which can be written as

$$\mathbf{R}_{2,3,t+dt} = \Delta\mathbf{R}\mathbf{R}_{2,3,t}. \tag{6}$$

Where

$$\Delta\mathbf{R} = \mathrm{I} + \sin\varphi(\mathbf{u}\times) + (1-\cos\varphi)(\mathbf{u}\times)^2 \tag{7}$$

is the Euler-Rodrigues formula for axis angle rotations. $\mathrm{u}\times$ is cross product matrix of unit vector $\mathbf{u}$. $(\mathbf{u}\times)^2$ is the skew matrix [32]. If we define the angular velocity of cylinder at time t as $\boldsymbol{\omega}_t$, $\varphi = |\omega_t dt|$ is the rotation angle around the axis $\mathrm{u} = \omega_t / |\omega_t|$. When $|\omega_t| = 0$, $\mathbf{u}_{t+dt} = \mathbf{u}_t$ and the orientation is at equilibrium.

#164286 - $15.00 USD Received 7 Mar 2012; revised 3 May 2012; accepted 4 May 2012; published 24 May 2012

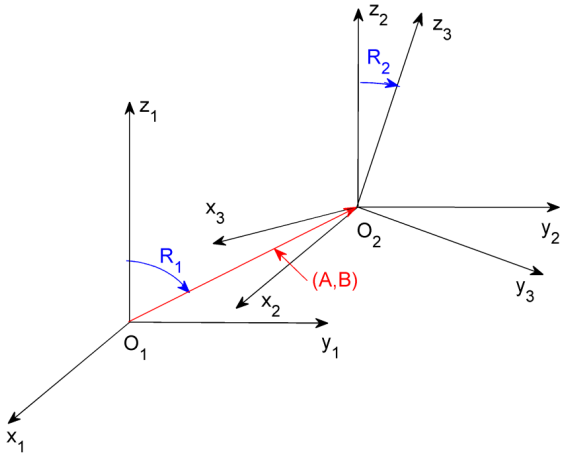

Fig. 2. Rotations and translations of beam coefficients from initial Cartesian coordinate system $x_1y_1z_1$ to an arbitrary coordinate system $x_3y_3z_3$ through translated coordinate system $x_2y_2z_2$. (**A**) and (**B**) are translations of beam coefficients along $\mathbf{O_1O_2}$ direction. $\mathbf{R_1}$ and $\mathbf{R_2}$ are rotations of beam coefficients.

2.3. Translation and rotation of micro- and nano-particles

A particle near the focal region, as a result of optical force and torque, will be forced to translate to an equilibrium position and rotate to a stable orientation. The force and torque efficiencies exerted on the particle, $\boldsymbol{Q}$ and $\boldsymbol{\tau}$, are calculated with optical tweezers computational toolbox [7], which uses sums of products of the expansion coefficients of incident and scattered fields (a_{nm}, b_{nm}, p_{nm} and q_{nm}) to calculate the change in linear momentum. The force and torque acting on the particle, currently in normalized form, can be converted to SI with

$$\mathbf{F} = \frac{n_m P_{\text{inc}} \mathrm{Q}}{c}, \tag{8}$$

$$\mathbf{\Gamma} = \frac{P_{\text{inc}} \boldsymbol{\tau}}{\omega}. \tag{9}$$

Where n_{m} is refractive index of medium, P_{inc} is the incident power of laser beam, and ω is the optical frequency.

The dynamic simulation model is also based on hydrodynamic equations. For a particle at low Reynolds number, when an exerted force is removed, it will take less than a few microseconds to slow to the flow speed [33]. Our calculations are in the regime of low Reynolds number, therefore, we consider that the viscous drag exerted opposes the optical force, and that the viscous torque opposes the radiation torque. So we can write $\mathrm{F}_{\text{drag}} = -\mathrm{F}$ and $\Gamma_{\text{drag}} = -\Gamma$, by Newton's third law of motion.

The effect of force and torque exerted on a particle are obtained with the following equations, which is based on computing the particle's next position and orientation a short time interval later. Given the force, torque, position and orientation at time t, the equations of motion we solve for a particle are

$$\boldsymbol{v} = \boldsymbol{\gamma}_{\text{t}}^{-1}\mathbf{F}, \tag{10}$$

$$\boldsymbol{\omega} = \boldsymbol{\gamma}_{\text{r}}^{-1}\mathbf{\Gamma}, \tag{11}$$

#164286 - $15.00 USD Received 7 Mar 2012; revised 3 May 2012; accepted 4 May 2012; published 24 May 2012

$$\boldsymbol{r}(t+\mathrm{d}t)=\boldsymbol{r}(t)+\boldsymbol{v}\mathrm{d}t, \tag{12}$$

where $\boldsymbol{\gamma_t}$ and $\boldsymbol{\gamma_r}$ are the translational and rotational friction tensors for a particle [34], and $\boldsymbol{r}$ is the position of the center of the object. Since the translational and rotational friction tensors given by Delatorre and Bloomfield [34] only apply to elongated cylinders (aspect ratio > 1), we did not perform calculations for disks (aspect ratio < 1).

$$\mathrm{d}t=\frac{\alpha}{P_{\mathrm{inc}}(1+\beta|\boldsymbol{\omega}_t|)} \tag{13}$$

is an asymptotic dynamic time step, depending on the incident power of laser beam and angular velocity of the particle. α and β are constants, but they can be changed for different cylinders and different beams. New orientations can be obtained by Eq. (6). Based on this model, we can dynamically simulate the motion of micro- and nano-structures near the focal region. By changing the starting position and orientation, we can exclude local minima from the simulation.

3. Results

The trapping and rotation dynamics of cylindrical structures was determined from Eqs. (8) – (9). The laser beam we used in the calculations was a single tightly focused Gaussian beam, focused by high numerical aperture lens (NA = 1.25). The beam propagates along the z_1 direction with its focus located at $(x_1, y_1, z_1) = (0, 0, 0)$. The wavelength of the beam was λ_0 = 1064 nm in vacuum and λ = 800 nm in water, the power of the beam going through the focal plane was P_{inc} = 1 mW. The immersed cylinder was made of common glass with a refractive index n_{p} = 1.57. The origin of the cylinder was located at the centre of mass.

A glass nanowire with diameter of 50 nm and length of 2000 nm has been simulated using dynamic simulation model. Figure 3 shows the trajectories of the nanowire as functions of time in linearly polarized and circularly polarized beams. The nanowire was trapped at (0, 0, $-0.03)\lambda$ in a linearly polarized beam and at (0, 0, $-0.1)\lambda$ in a circularly polarized beam. For some particles, the equilibrium position is possibly before the focal plane [35]. That is, the center of the particle is before the focal plane (but part of the particle lies beyond the focal plane as well). The nanowire orients with a tilt angle φ = 86.6 degrees in the linear polarized beam, but along the beam axis in the circularly polarized beam. Differences between the final orientations of the nanowire in beams of different polarisations mean that the polarisation of focused laser beam plays an important role in optical trapping of the nanowire.

The microcylinder in Fig. 1 and nanowire in Fig. 3 behave in very different manners. In a linearly polarised beam, the microcylinder is trapped along the beam axis, whereas the nanowire is trapped with a large tilt angle (φ = 86.6 degrees). Nanowire orientation is sensitive to polarisations, it is therefore reasonable to believe that the nanowires and microcylinders with other sizes may also be trapped with different orientations both in linearly and circularly polarized beams. Knowing this behavior is crucial when considering using such a particle as a probe. A cylinder's size and the beam polarisation change the equilibrium orientation. We look at stable orientations of micro- and nano-cylinders with diameters less than 500 nm and lengths less than 3000 nm. Figure 4 shows the orientation landscapes for these nanowires and microcylinders trapped in linearly and circularly polarized beams. There are four regimes in the orientation landscapes for cylinders with aspect ratio larger than one: an untrapped region, vertical region, horizontal region, and an intermediate region between the vertical and horizontal regions. In general, larger cylinders can't be trapped. The cylinders in vertical and horizontal regions are trapped along the beam axis and transverse to the beam axis respectively. The intermediate region is the region where a cylinder can be trapped with a tilt angle between 0 and 90 degrees from the beam axis.

#164286 - $15.00 USD Received 7 Mar 2012; revised 3 May 2012; accepted 4 May 2012; published 24 May 2012

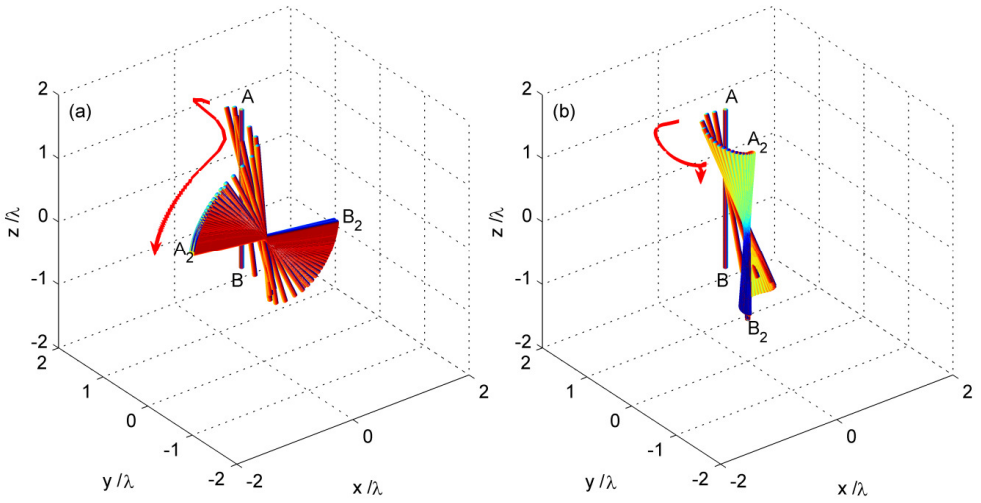

Fig. 3. Trajectories of a simulated glass nanowire with D = 50 nm and L = 2000 nm in (a) linearly and (b) circularly polarized beams. AB is initial position and orientation of the nanowire, A_2B_2 is the trapped position and orientation. The solid curve and arrow show the trajectory of one top center of the cylinder. The linear polarisation contributed to the horizontal torque component which would make the nanowire lie down. But the circular polarisation made the time-averaged horizontal torque component so weak that the nanowire could stand up.

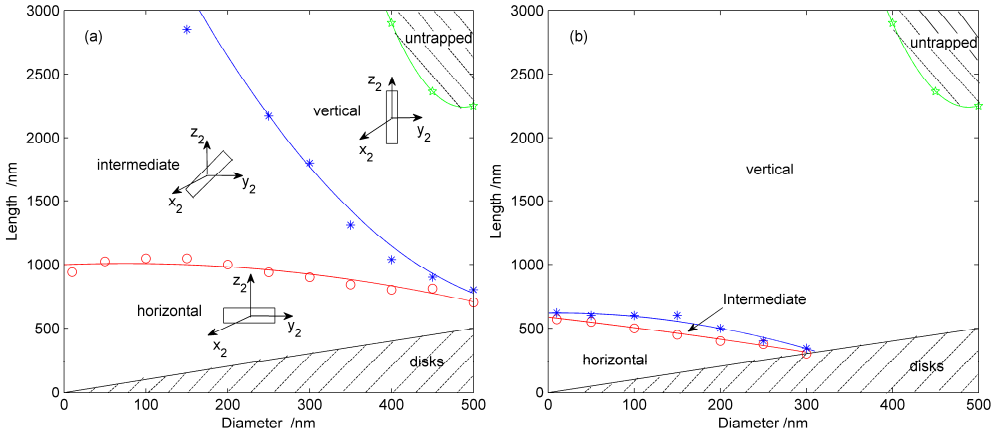

Fig. 4. Orientations landscapes of nanowires and microcylinders in (a) linearly polarized and (b) circularly polarized beams. The coordinate system is Cartesian coordinate system centred at cylinder position. The rectangular shapes in (a) show the orientations of cylinders in each region. Four regimes in the orientation landscapes are the untrapped region, vertical region, horizontal region, and the intermediate region between the vertical and horizontal regions. The "circle" means the longest nanowire or microcylinder trapped horizontally for each diameter. The "asterisk" represents the shortest nanowire or microcylinder trapped vertically for each diameter. The "star" indicates the longest nanowire or microcylinder for each diameter, which can be trapped (vertically). The fitting curves are used to distinguish different regions.

There is a big difference between the orientation landscapes of cylinders trapped with beams of different polarisations. The vertical region is larger for circular polarisation and the intermediate and horizontal regions become smaller when compared to corresponding regions for linear polarisation. This means that the rods trapped with stable horizontal orientation or

#164286 - $15.00 USD Received 7 Mar 2012; revised 3 May 2012; accepted 4 May 2012; published 24 May 2012

with a tilt angle in linear polarisation may be trapped with vertical orientation in a circularly polarized beam. A similar strong dependence on polarization has been noted for non-conservative forces on nanoparticles [36], and it is possible that such forces contribute here. However, our T-matrix method only gives the total force, rather than conservative and non-conservative components separately, so this remains an interesting open question. However, the untrapped region doesn't change from linearly to circularly polarized beams. Polarisation is therefore not a key factor to determine whether a particle can be trapped or not.

The torque efficiencies of cylinders with diameters of 300 nm with different lengths were calculated as functions of tilt angle from the beam axis and are shown in Fig. 5. The lengths of cylinders depicted are 600, 1200 and 1800 nm. This calculation was performed for cylinders located at equilibrium positions in the polarisation plane of a linearly polarized beam. In the circularly polarized beam, the plane of tilt is simply a plane parallel to the beam axis. The torque efficiency, $Q_{\tau t,}$ is the torque in these planes. When $Q_{\tau t} < 0$ the orientation angle decreases and increases when $Q_{\tau t} > 0$. A stable orientation is achieved when a deviation either side of $Q_{\tau t} = 0$ returns the object its previous orientation. According to the curves shown in Fig. 5, one can obtain the stable orientations of these cylinders. The cylinder with length of 600 nm orients horizontally ($\varphi = 90°$) in a linearly polarized beam, but vertically ($\varphi = 0°$) in a circularly polarized beam. The cylinder with length of 1200 nm orients with a tilt angle $\varphi = 43$ degrees in a linearly polarized beam, but vertically in a circularly polarized beam. The cylinder with length of 1800 nm is aligned vertically both in a linearly polarized beam and in a circularly polarized beam. According to our calculation, shorter cylinders are stably aligned transverse to the beam axis, whereas longer cylinders dispose themselves toward the beam axis. This behavior is consistent with other theoretical predictions for particles with linear structures subjected to tightly focused laser beams [26]. In the intermediate region, cylinders may orient to quite different orientations with small changes in their dimensions and material. The results demonstrate that the polarisation of focused laser beam plays an important role the stable orientation of a cylinder.

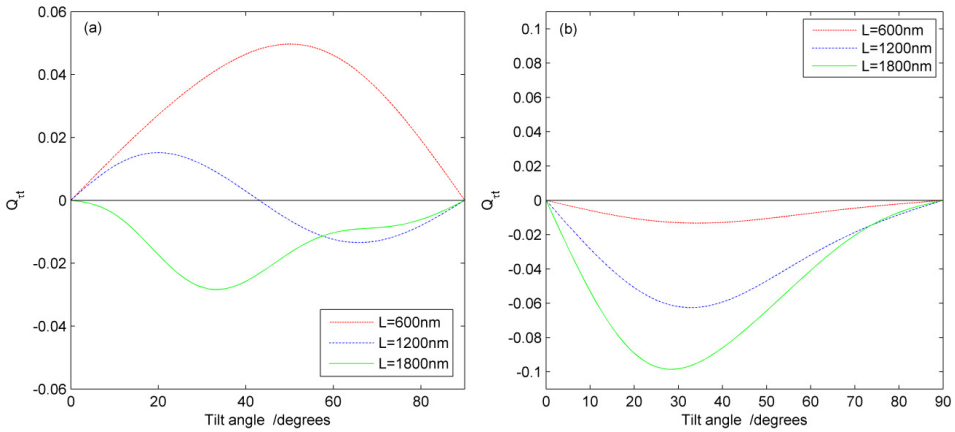

Fig. 5. Torque efficiencies, $Q_{\tau t,}$ for cylinders with diameter of 300 nm and different lengths located in polarisation plane of (a) a linearly polarized beam and in a plane parallel to the beam axis in (b) a circularly polarized beam as a function of tilt angle.

4. Conclusions

The translation and rotation of microcylinders and nanowires have been studied under dynamic simulation. Dynamic modelling can show how an object (such as the cylinders discussed here) will travel and rotate as they find equilibrium positions and stable orientations. We have shown a range of microcylinders and nanowires which can be stably trapped and rotate in the single tightly focused Gaussian beam. A microcylinder with

#164286 - $15.00 USD Received 7 Mar 2012; revised 3 May 2012; accepted 4 May 2012; published 24 May 2012

diameter of 500 nm and length of 2000 nm at different starting positions and orientations is trapped at the same equilibrium position along the beam axis. A nanowire with diameter of 50 nm and length of 2000 nm has been simulated, showing that it can be trapped with a large tilt angle in a linearly beam and along the beam axis in a circularly polarized beam and may rotate with handedness of polarisation. The orientation landscapes of glass cylinders with diameters between 0 and 500 nm and lengths between 0 and 3000 nm have been presented. There are four regimes in the orientation landscapes of glass cylinders: an untrapped region, vertical region, horizontal region, and an intermediate region between the vertical and horizontal regions. The orientation landscapes of the cylinders demonstrate that the stable orientations of cylinders can strongly depend on the trapping beam polarisation. The torque efficiencies on cylinders with diameter D = 300 nm with different lengths in linearly polarized and circularly polarized beams have been calculated. The orientations of microcylinders and nanowires depend on the competition between polarisation and gradient force. Apart from these specific results for cylindrical particles, including nanowires, it is important to realise that the method is quite general, and can be used to find equilibrium positions and orientations for any particle for which the optical force can be calculated. Ideally, it should also be possible to calculate the translational and rotational viscous drag tensors, and coupling tensors between rotation and translation as can be required for chiral particles and linear structures near an interface [37].

However, if the particle falls into an equilibrium position in the trap, it is possible to approximate these drag tensors very simply by using the tensors for a sphere. In this case, the trajectories will not be correct, but the final equilibrium position will be. In the case that the particle does not reach an equilibrium position and orientation, but instead approaches a steady-state cyclic trajectory, this trajectory will be affected by approximations made in these tensors. Even with these limitations, the method presented in this paper provides a useful method for the determination of equilibrium positions of many kinds of particles. More generally, the method used here can be used to simulate the motion, both translational and rotational, of many kinds of particles in optical traps. For future work, we are interest in the investigation of translation and rotation of other geometries and materials, and demonstrating their applications based on their properties.

Acknowledgments

This work was supported by the Australian Research Council.

#164286 - $15.00 USD Received 7 Mar 2012; revised 3 May 2012; accepted 4 May 2012; published 24 May 2012